Journal of Computer Assisted Tomography
15(4):621–628, July/August

Pharmacokinetic Parameters in CNS Gd-DTPA Enhanced MR Imaging

Gunnar Brix, Wolfhard Semmler, Rüdiger Port, Lothar R. Schad, Günter Layer, and Walter J. Lorenz

Abstract: Dynamic MR imaging can be used to study tissue perfusion and vascular permeability. In the present article a procedure for dynamic MR is presented, which (a) accurately resolves the fast kinetics of tissue response during and after intravenous infusion of the paramagnetic contrast medium Gd-DTPA and (b) yields a linear relationship between the measured MR signal and the Gd-DTPA concentration in the tissue. According to these features, the measured signal-time curves can be analyzed within the framework of pharmacokinetic modeling. Tissue response has been parameterized using a linear two-compartment open model, with only negligible effects of the peripheral compartment on the central compartment. The three model parameters were fitted to the signal-time data pixel by pixel, based on a set of 64 rapid SE images (SE 100/10 ms, image scan time 13 s, interscan intervals 11 s). This makes it possible to construct parameter images, whereby structures become visible that cannot be distinguished in conventional Gd-DTPA enhanced MR. As a clinical example, the approach is discussed in a case of glioblastoma. **Index Terms:** Magnetic resonance imaging, techniques—Contrast media—Tissue perfusion—Magnetic resonance imaging, physics and instrumentation.

Magnetic resonance imaging, with its good soft tissue contrast, is the foremost imaging method for detecting pathological processes of the CNS. Nevertheless, with MR it is frequently difficult to distinguish between different brain lesions, for example, between benign and malignant neoplasms or between tumor and perifocal edema. The application of the paramagnetic contrast medium (CM) Gd-DTPA has considerably improved the sensitivity and specificity of MR. Gadolinium-DTPA enhanced MR has therefore become the method of choice for diagnostic imaging of many CNS disorders (1).

It should be emphasized, however, that routinely performed Gd-DTPA enhanced MR only provides a static impression of the signal enhancement and does not make use of the kinetic properties of the MR signal variation. This additional dimension of information can be attained by dynamic MR. From dynamic CT it is well known that density-time curves measured after intravenous injection of an ionic or nonionic CM can be useful in differential diagnosis and furthermore can provide functional information on vascular permeability and blood–brain barrier (BBB) integrity (2–6). Dynamic MR should lead to even better results, since the degree of MR signal enhancement is often greater than that seen with CT (7). The lack of radiation risk is a further advantage of MR. In a study with 17 patients, Koschorek et al. (8) found different signal-time curves after intravenous bolus injection of Gd-DTPA for gliomas, paragliomas, tumors of mesodermal origin, and arteriovenous malformations. In this study, however, the signal-time courses (10 data points) of regions of interests (ROIs) were analyzed only by fitting straight lines to the wash-in and wash-out phases.

It was the aim of our investigation to provide a method for dynamic MR, which (a) accurately resolves the fast kinetics of tissue response after intravenous administration of Gd-DTPA and (b) yields a description of the measured signal-time curves in terms of pharmacokinetic parameters. The signal-time curves were analyzed pixel by pixel

From the Institut für Radiologie und Pathophysiologie, Deutsches Krebsforschungszentrum, Postfach 101949, W-6900 Heidelberg, Germany. Address correspondence and reprint requests to Dr. rer. nat. G. Brix.

to preserve the spatial information of the MR images. The results will be presented as synthetic parameter images revealing additional structures of the lesion that cannot be seen in conventional Gd-DTPA enhanced MR.

THEORY

Gadolinium affects the MR signal mainly by proton relaxation enhancement. The MR signal variation, therefore, can be parameterized for any given MR pulse sequence provided that (a) the relationship between Gd-DTPA concentration and proton relaxation times T1 and T2 is known and (b) the concentration of the CM in the tissue can be described on the basis of a suitable pharmacokinetic model (9).

Proton Relaxation Enhancement

In aqueous solutions of paramagnetic ions, the most important mechanism for enhancing the relaxation of water protons is the dipole-dipole interaction between the large magnetic moment of paramagnetic ions and the magnetic moment of water protons. In accordance with the Solomon-Bloembergen equations (10,11), a linear relationship between paramagnetic ion concentration and relaxation rates, $R1 = 1/T1$ and $R2 = 1/T2$, was found experimentally (12) for dilute solutions of Cr^{3+}, Mn^{2+}, Ni^{2+}, Cu^{2+}, and Gd^{3+}. The same relation was found to be valid for aqueous solutions of Gd-DTPA (13,14). Moreover, empirical data suggest that even in blood and soft tissues, the bulk or average relaxation rates are proportional to the Gd-DTPA concentration in the tissue (14–17). A further discussion of the last point is given in a review by Rosen et al. (9) published in 1989.

Thus, it is assumed that the local tissue relaxation times $T1_{CM}$ and $T2_{CM}$ are related to the local tissue Gd-DTPA concentration C_{CM} by the equations

$$\frac{1}{T1_{CM}} = \frac{1}{T1_0} + \alpha C_{CM} \qquad (1a)$$

$$\frac{1}{T2_{CM}} = \frac{1}{T2_0} + \beta C_{CM} \qquad (1b)$$

where $T1_0$ and $T2_0$ are the intrinsic relaxation times of the tissue measured in the absence of the CM and α and β are tissue- and frequency-dependent constants.

Plasma Kinetics of Gd-DTPA (15,18–21)

After intravenous injection, Gd-DTPA plasma concentrations decline biexponentially; mean half-lives of 0.20 ± 0.13 h (distribution phase) and 1.58 ± 0.13 h (elimination phase) have been determined in healthy volunteers at doses of 0.1 and 0.25 mmol/kg body weight (20). The main route of elimination is renal excretion; there is no indication of any metabolism. The total distribution volume of Gd-DTPA corresponds to the volume of extracellular body water (20). Gadolinium-DTPA does not cross the intact BBB, owing to its high molecular weight, its charge, and its extreme hydrophilicity (21). In contrast, it readily enters into brain tumors where the BBB is locally defective.

Pharmacokinetic Modeling

In our dynamic MR measurements, the signal enhancement by Gd-DTPA is observed only during the first 24 min after the beginning of the infusion. Within this time range, Gd-DTPA plasma kinetics can satisfactorily be described with a linear one-compartment open model. When reanalyzing the data of Weinmann et al. (22) (10 individual concentration-time courses) for this time range, we found relative residuals ($| C_p - C_m | / C_m$) between predicted (C_p) and measured (C_m) plasma concentrations of up to 12.3% (mean 4.6%) with the one-compartment model, as compared with a maximum value of 7.9% (mean 2.2%) with the biexponential model originally used. We therefore used a linear one-compartment open model with zero-order input to describe the Gd-DTPA in plasma. The model was perfected by incorporating the extracellular space of the lesion as a peripheral compartment (no. 2), which is connected to the central (plasma) compartment (no. 1) by linear exchange processes in both directions (Fig. 1). The mass balances for this model can be expressed by the following two differential equations (23,24):

$$\frac{dM_1}{dt} = K_{in} - (k_{12} + k_{el})\, M_1 + k_{21} M_2 \qquad (2a)$$

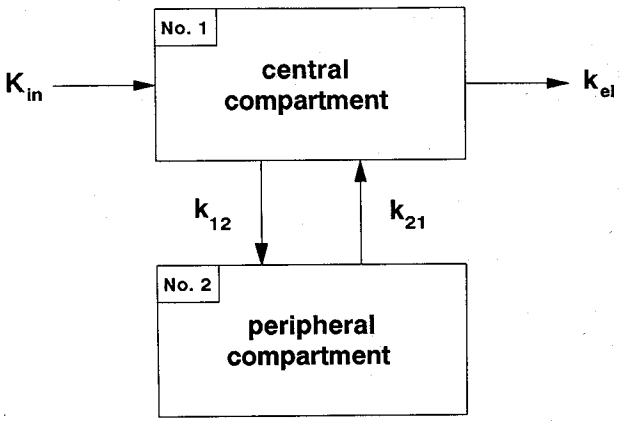

FIG. 1. Open two-compartment model with constant rate infusion. Elimination occurs only from the central compartment.

$$\frac{dM_2}{dt} = k_{12}M_1 - k_{21}M_2 \quad (2b)$$

M_1 and M_2 are the amounts of Gd-DTPA in compartment nos. 1 and 2, k_{12} is the first-order rate constant (time^{-1}) for transfer of Gd-DTPA from compartment no. 1 to compartment no. 2, k_{21} is the rate constant in the opposite direction, k_{el} is the first-order rate constant for elimination of Gd-DTPA from compartment no. 1, and K_{in} is the zero-order rate constant that is equal to the Gd-DTPA infusion rate (mass/time). If the transfer velocity of the Gd-DTPA complex between the two compartments is equal in both directions, the rate constants k_{12} and k_{21} are related by the equation $k_{12}\,V_1 = k_{21}\,V_2$, where V_1 and V_2 are the volumes of the central and the peripheral compartment, respectively. To consider different binding and trapping of the CM within the two compartments, this simplification is not used in the following equations.

Assuming that there is no active Gd-DTPA accumulation in a lesion and that its distribution volume V_2 is insignificant with respect to the volume of the central compartment, Eq. 2a can be simplified by neglecting the terms $k_{12}\,M_1$ and $k_{21}\,M_2$. By setting the concentrations $C_1 = M_1/V_1$ and $C_2 = M_2/V_2$, we obtain, on rearranging,

$$\frac{dC_1}{dt} = \frac{K_{in}}{V_1} - k_{el}C_1 \quad (3a)$$

$$\frac{dC_2}{dt} = \frac{V_1}{V_2}k_{12}C_1 - k_{21}C_2 \quad (3b)$$

This decoupled system of differential equations can now be solved successively. With the initial conditions $C_1(0) = 0$ and $C_2(0) = 0$, the integration yields

$$C_1(t) = \frac{K_{in}}{V_1 k_{el}}[\exp(k_{el}t') - 1]\exp(-k_{el}t) \quad (4a)$$

$$C_2(t) = \frac{K_{in}k_{12}}{V_2}\{v[\exp(k_{el}t') - 1]\exp(-k_{el}t) - u[\exp(k_{21}t') - 1]\exp(-k_{21}t)\} \quad (4b)$$

with $u = [k_{21}(k_{21} - k_{el})]^{-1}$ and $v = [k_{el}(k_{21} - k_{el})]^{-1}$. During the Gd-DTPA infusion ($0 \leq t \leq \tau$), the identity $t' = t$ has to be used, afterwards the identity $t' = \tau$.

Assuming that the infused CM is instantly mixed throughout the plasma volume, with Eq. 4b the Gd-DTPA concentration in the extracellular space of the lesion is parameterized in terms of a simple pharmacokinetic model. If the lesion is inhomogeneous, it has to be divided into different approximately homogeneous parts, e.g., into tumor and perifocal edema. This can be done either by an ROI technique or by a pixel by pixel analysis of the dynamic MR images. In this case each region or voxel of the lesion has to be considered as a separate peripheral compartment, which independently interacts with the central compartment; interactions between neighboring peripheral compartments are neglected.

Gd-DTPA Enhanced SE Signal

In the absence of a paramagnetic CM, the MR signal S_0 for a conventional SE sequence can be described by

$$S_0 = k\,\rho\exp\left(\frac{-TE}{T2_0}\right)\left[1 - \exp\left(\frac{-TR}{T1_0}\right)\right] \quad (5)$$

where ρ is the proton density, TE the SE time, TR the sequence repetition time, and k an arbitrary constant. If the tissue contains Gd-DTPA, the bulk relaxation times $T1_{CM}$ and $T2_{CM}$ defined by the relations 1a and 1b have to be used in Eq. 5 in place of the intrinsic values $T1_0$ and $T2_0$:

$$S_{CM} = k\rho\exp\left(\frac{-TE}{T2_0}\right)\exp(-TE\,\beta\,C_{CM})\left[1 - \exp\left(\frac{-TR}{T1_0}\right)\exp(-TR\,\alpha\,C_{CM})\right] \quad (6)$$

For dynamic MR, the SE sequence parameters TR and TE should be chosen as short as possible to guarantee an adequate time resolution and an acceptable signal/noise ratio, respectively. Assuming that the conditions $TR\,\alpha\,C_{CM} << 1$ and $TE\,\beta\,C_{CM} << 1$ are fulfilled for the sequence parameters taken in the measurement (e.g., TR = 100 ms, TE = 10 ms), the linear approximations

$$\exp(-TR\,\alpha\,C_{CM}) \approx 1 - TR\,\alpha\,C_{CM} \quad (7a)$$

$$\exp(-TE\,\beta\,C_{CM}) \approx 1 - TE\,\beta\,C_{CM} \quad (7b)$$

can be used in Eq. 6. In this approximation, a linear relationship between the local tissue Gd-DTPA concentration C_{CM} and the enhanced MR signal S_{CM} is obtained,

$$S_{CM} = S_0(1 + F\,C_{CM}) \quad (8)$$

where F is a multidimensional function depending on TR, TE, $T1_0$, $T2_0$, α, and β. Although the linear approximation seems to be quite reasonable for the usual Gd-DTPA dose of 0.1 mmol/kg body weight, its accuracy has to be validated experimentally. Note that Eq. 8 is also derived, if the more exact SE signal equation (14) is used instead of Eq. 5.

Finally, by using the linear relation $C_{CM} = f_{ex}\,C_2$ between the bulk tissue Gd-DTPA concentration C_{CM} and the Gd-DTPA concentration C_2 in the extracellular space of the tissue (where f_{ex} is the frac-

tion of the extracellular volume), an explicit expression for the time-dependent Gd-DTPA enhanced MR signal $S_{CM}(t)$ is obtained:

$$\frac{S_{CM}(t)}{S_0} = 1 + A\{v[\exp(k_{el}t') - 1]\exp(-k_{el}t) - u[\exp(k_{21}t') - 1]\exp(-k_{21}t)\} \quad (9)$$

where A is a constant depending on the properties of the tissue ($T1_0$, $T2_0$, α, β, k_{12}, V_2, f_{ex}), of the sequence used (TR, TE), and of the infusion rate (K_{in}). As already mentioned, during the Gd-DTPA infusion ($0 \leq t \leq \tau$), the identity $t' = t$ has to be used, afterwards the identity $t' = \tau$. It is a remarkable property of the deduced Model Eq. 9 that, apart from multiplication by the multidimensional amplitude A, the shape of the temporal response $S_{CM}(t)/S_0$ is determined—in the approximation discussed—only by the kinetic parameters k_{21} and k_{el}.

MATERIALS AND METHODS

Instrumentation

The measurements were performed on a Magnetom SP (Siemens, Erlangen, F.R.G.) superconducting whole-body MR imager operating at 64 MHz. The MR computer (MicroVAX II; DEC, Maynard, MA, U.S.A.) was connected directly (Ether-Net; DEC) to an external computer (MicroVAX 3500; DEC), where the software for the iterative parameter calculation developed by our group was implemented. The paramagnetic CM Magnevist (Schering, Berlin, F.R.G.) was injected using a variable speed infusion pump Doltron PIM 717 (Doltron AG, Uster, Switzerland).

Imaging Protocol

A series of 64 rapid SE brain images (SE 100/10 ms, image scan time 13 s, interscan intervals 11 s) was taken in a slice with best visualization of the lesion using a head coil with an internal diameter of 30 cm. The matrix size was 128 × 128 with a nominal voxel size of about 1.7 × 1.7 × 10 mm^3. After data acquisition the matrix size was interpolated to 256 × 256. The total measurement time was 25.6 min. A total dose of 0.1 mmol Gd-DTPA/kg body weight was administered intravenously by constant rate infusion within 4 min. Infusion was started simultaneously with the measurement of the fifth SE image. Furthermore, two series of SE images (SE 2,000/34,68,102,136 ms and SE 600/34,68,102;136 ms) were acquired in the same slice immediately before and after dynamic MR using multiecho sequences.

Data Analysis

Based on a set of $N = 64$ dynamic MR images, the three parameters k_{21}, k_{el}, and A of Eq. 9 were fitted pixel by pixel by minimizing the sum Q of square deviations between the experimental data L_i and the calculated fit values $S_{CM,i}$ ($1 \leq i \leq n$):

$$Q = \sum_{i=1}^{N} (S_{CM,i} - L_i)^2 \quad (10)$$

The computation was done iteratively using the Marquart algorithm for least squares estimation of nonlinear parameters (25). To establish whether the measured signal-time curve of a given voxel showed a signal enhancement, the maximum S_{max} of the fit curve was calculated. For $(S_{max} - S_0) \geq 4\sqrt{Q/(N-1)}$, the estimated parameters were stored in the corresponding parameter images. To limit the computing time, the pixel-oriented analysis was performed only in an ROI that amply surrounded the image area that shows a signal enhancement. After computation, the parameter images were displayed either at the MicroVAX 3500 color graphic display or at the MR console. Pre- and postcontrast relaxation time images were computed on the basis of the measured pre- and postcontrast multiecho image series using the software available at the imager.

CASE STUDY

Dynamic MR was performed in a 60-year-old woman with a recurrence of a glioblastoma. The histological diagnosis was known from previous surgery.

Figure 2 shows 4 of 64 dynamic MR images (SE 100/10 ms); the first was acquired prior to, the second 4 min after, the third 14 min after, and the last one 24 min after the onset of constant rate infusion of 4 min duration. Mappings of the estimated tissue specific parameters k_{21} and A are given in Fig. 3a and b. For comparison, T1-weighted SE images (SE 600/34 ms) measured immediately before and after acquisition of the dynamic MR data set are displayed in Fig. 3c and d. In the precontrast image (Fig. 3c), the tumor is slightly hypointense as compared with the surrounding normal brain tissue. After Gd-DTPA application (Fig. 3d), an inhomogeneous enhancement with ill defined margins is observed in the tumor tissue. The central hypointense areas are interpreted as necrosis. The well defined contrast enhanced rim (left lateral) is due to meningeal involvement. In the parameter images (Fig. 3a and b), the internal structure of the tumor is much more apparent than in the pre- and postcontrast images. Furthermore, the rapid and strong en-

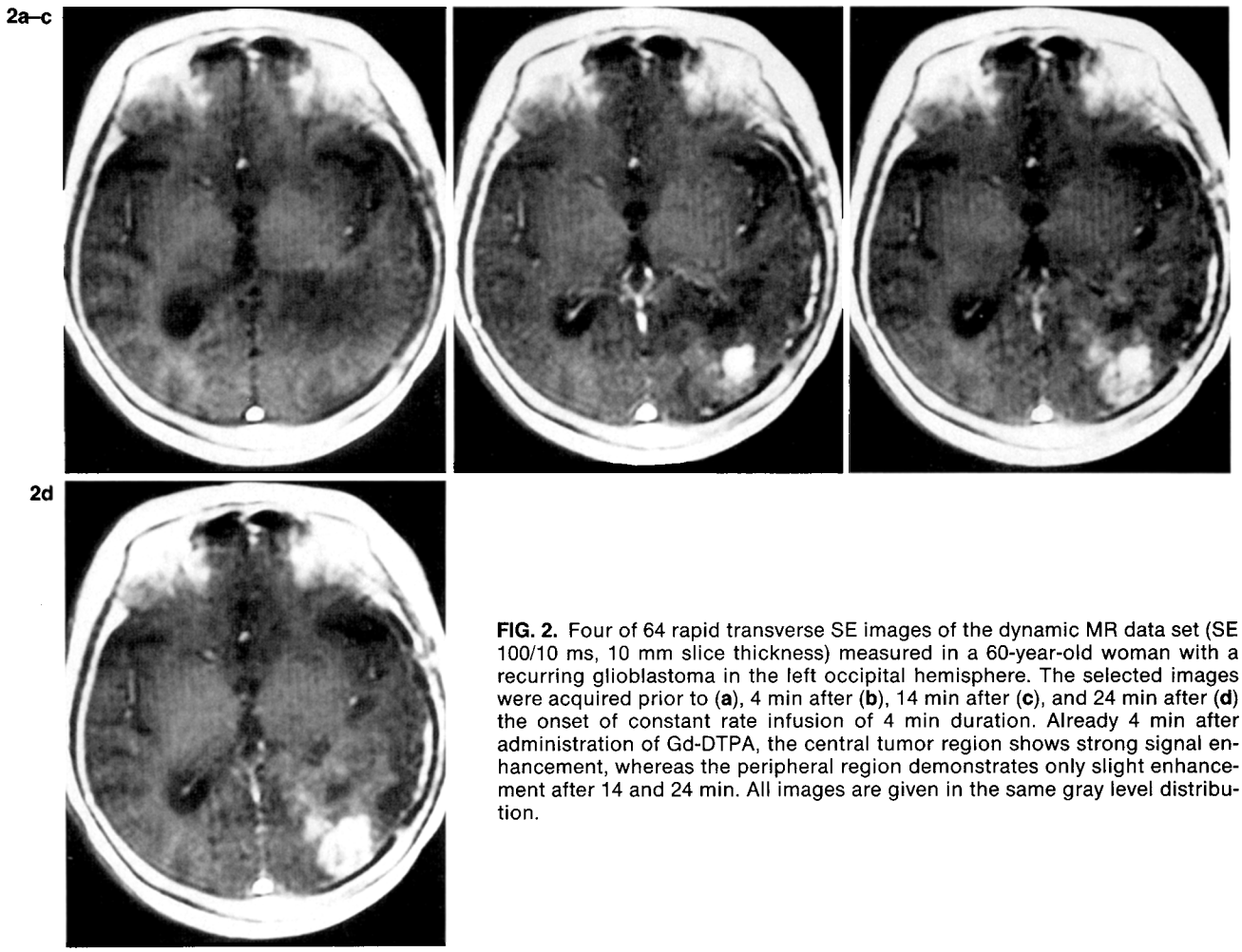

FIG. 2. Four of 64 rapid transverse SE images of the dynamic MR data set (SE 100/10 ms, 10 mm slice thickness) measured in a 60-year-old woman with a recurring glioblastoma in the left occipital hemisphere. The selected images were acquired prior to (**a**), 4 min after (**b**), 14 min after (**c**), and 24 min after (**d**) the onset of constant rate infusion of 4 min duration. Already 4 min after administration of Gd-DTPA, the central tumor region shows strong signal enhancement, whereas the peripheral region demonstrates only slight enhancement after 14 and 24 min. All images are given in the same gray level distribution.

hancing central part of the tumor exhibits an additional internal structure (Fig. 3a), which cannot be seen in the conventional Gd-DTPA enhanced image (Fig. 3d). The physiological enhancement of the choroid plexus in the compressed left ventricle is clearly shown in the parameter images; the high intensities of the amplitude image and of the k_{21} rate image reflect the high perfusion of the choroid plexus.

Signal-time curves of two representative ROIs—one in the right part of the fast and strong enhancing central region of the tumor (23 pixels) and one in the surrounding tumor region (19 pixels)—are presented in Fig. 4. The fitting routine yielded $A = 2.54 \pm 0.02$ a.u., $k_{21} = 2.59 \pm 0.18$ min^{-1} ($T_{21} = 0.267$ min), and $k_{el} = 0.0236 \pm 0.0006$ min^{-1} ($T_{el} = 29.4$ min) for the central tumor region and $A = 0.82 \pm 0.02$ a.u., $k_{21} = 0.734 \pm 0.081$ min^{-1} ($T_{21} = 0.944$ min), and $k_{el} = -0.0156 \pm 0.0017$ min^{-1} ($T_{el} = -44.4$ min) for the surrounding tumor tissue. The values given in parentheses are half-lives, i.e., $T_{21} = \ln(2)/k_{21}$ and $T_{el} = \ln(2)/k_{el}$. Based on the analyzed signal-time curves and the pre- and postcontrast relaxation time images, the largest differences between pre- and postcontrast relaxation rates were estimated according to Eq. 1a and 1b to be $\Delta R1 < 0.0015$ s^{-1} and $\Delta R2 < 0.001$ s^{-1}. Thus, the error in the approximations 7a and 7b is <1.3% for TR = 100 ms and <0.005% for TE = 10 ms, respectively.

DISCUSSION

Dynamic MR is presently being investigated for possible clinical applications by many MR research groups. The main goal is to study tissue perfusion and vascular permeability, which may be useful in differential diagnosis, therapy planning, and therapy follow-up. The crux, however, is that the CM is frequently administered in an undefined way by bolus injection. Assuming a typical injection time between 10 and 30 s, this means that the CM is injected within a time that is on the same order of magnitude as the wash-in time of many CNS lesions. Thus, the observed tissue response is significantly determined by the way in which the Gd-

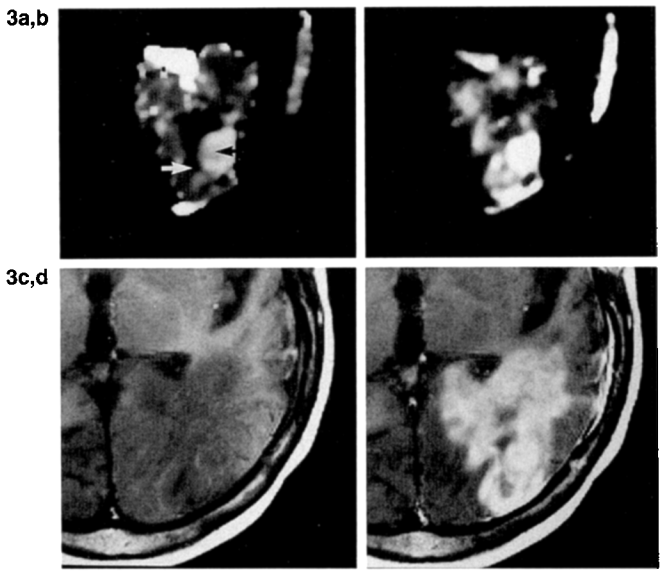

FIG. 3. The k_{21} parameter image **(a)** and the amplitude parameter image **(b)** computed from the dynamic MR data set presented in part in Fig. 2. To display the whole k_{21} range adequately, the k_{21} image is presented in a logarithmic scale, i.e., $\log(1 + k_{21})$. For comparison, diagnostic pre- **(c),** and postcontrast **(d)** transversal T1-weighted SE images (SE 600/34 ms, 5 mm slice thickness) of the same slice are shown. The tumor in the left occipital hemisphere appears in the precontrast T1-weighted image (c) as a slightly hypointense lesion. After administration of Gd-DTPA, a strong signal enhancement takes place in the central part of the tumor, whereas in the peripheral region only a slight enhancement is observed (d). The margins of the tumor are ill defined in the postcontrast image. In the synthetic parameter images (a and b), the internal structure of the tumor is much more apparent than in the conventional pre- and postcontrast images. Furthermore, the fast and strong enhancing central tumor part exhibits an additional internal structure in the k_{21} image, which cannot be seen in the Gd-DTPA enhanced T1-weighted image. Note that the pixel-oriented analysis of the dynamic image set was performed only in a region of interest that surrounds the enhanced image region in the postcontrast T1-weighted image. Signal-time curves of two representative regions, which are marked by the arrows in (a), are given in Fig. 4.

DTPA is actually administered. In our investigation, this methodological problem has been circumvented by infusing the CM at a constant rate over 4 min instead of using a bolus injection. Hence, the measured signal-time curves can be analyzed as a response function to a well defined input function describing the administered Gd-DTPA dose as a function of time.

In the present article, a mathematical approach is presented that breaks the analysis of the signal-time curves into two parts: (a) an MR-specific part, in which the Gd-DTPA enhanced MR signal is connected to the Gd-DTPA concentration in the tissue, and (b) an MR-independent part, in which the Gd-DTPA concentration in the lesion is described by a pharmacokinetic model.

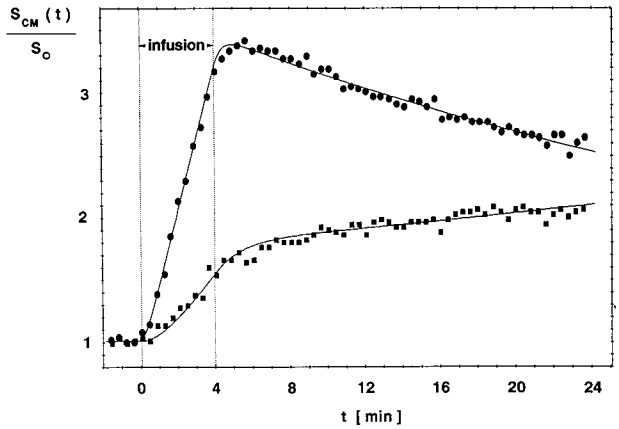

FIG. 4. Signal-time curves of two representative regions of interest. The upper curve represents the kinetic behavior of the right part of the rapid and strong enhancing central tumor region (black arrow in Fig. 3a), and the lower curve shows the kinetic behavior of the surrounding tumor tissue (white arrow in Fig. 3a). Estimates for the model-dependent parameter values are given in the text.

Gd-DTPA Enhanced SE Signal

A linear relationship between measured image signal and Gd-DTPA concentration in the tissue has been derived for the SE sequence based on the assumption that the conditions TR α $C_{CM} << 1$ and TE β $C_{CM} << 1$ are fulfilled for the sequence parameters chosen in the measurement. In the case of the examined glioblastoma, the analysis of the pre- and postcontrast relaxation times reveals that the conditions are well satisfied (TR α C_{CM} = TR $\Delta R1$ < 0.15, TE β C_{CM} = TE $\Delta R2 < 0.01$). Hence, in this case the error introduced by the linearization of the Signal Eq. 6 is <1.3%.

Although other MR sequences such as FLASH or FISP can be used for dynamic MR studies, they are handicapped by the fact that the relationship between measured MR signal and tissue Gd-DTPA concentration is given by a nonlinear function. It is a fundamental advantage of the SE as well as the inversion recovery sequence that the Gd-DTPA induced signal enhancement is (in the approximation discussed) directly proportional to the Gd-DTPA concentration in the tissue. The generally unknown MR tissue parameters T1, T2, α, and β only determine the proportionality factor.

In Vivo Mapping of Pharmacokinetic Parameters

To parameterize the Gd-DTPA concentration in a lesion, the distribution space of the lesion has been described as a peripheral compartment that is connected to a central (plasma) compartment by transport processes. The model-dependent transport parameters k_{12}, k_{21}, and k_{el} defined in Fig. 1 describe

the velocity of the CM transfer between the two compartments and the elimination of the CM from the central compartment, respectively. k_{el} is a systemic parameter, whereas k_{12} and k_{21} are tissue-specific transport parameters. In the CNS the extravasation of the CM into the extracellular space of the lesion results from changes in the integrity of the BBB, which normally renders cerebral capillaries impermeable to the CM (27).

As stated above, in our (as in any other) compartment model, a fast and perfect mixing of the CM within the plasma compartment is assumed. This means that the capillary blood flow is sufficient to replenish loss of the CM into the extracellular space of the lesion (26). In this limit, the rate of CM entry into the lesion depends only on vascular permeability, i.e., on the change or alteration of the BBB. In brain lesions with a less pronounced disruption of the BBB, such as multiple sclerosis plaques where the BBB alteration is produced by acute demyelination (26–28), the assumption is well fulfilled. On the other hand, regional blood flow may become a limiting factor if the BBB is completely absent. The analysis of the signal-time curve evaluated from the central tumor region of the glioblastoma, for example, has yielded a k_{21} value of 2.59 ± 0.18 min^{-1}. Such a fast signal enhancement ($T_{21} = 0.267$ min) may indeed be influenced in part by the local capillary blood flow. For the imaging clinician, however, this does not limit the relevance of the measured rate constant k_{21} characterizing both the perfusion and the vascular permeability of the lesion.

From the same central tumor region, a k_{el} value of 0.0236 min^{-1} was estimated, which is equivalent to a half-life of $T_{el} = 29.4$ min. This T_{el} lies within the range of one-exponential plasma half-lives that we calculated using the data of Weinmann (22), at 21–31 min for the first half hour after intravenous Gd-DTPA injection. On the other hand, from the surrounding tumor tissue, a half-life of $T_{el} = -44.4$ min was estimated, which is incompatible with a physiological interpretation of the assumed two-compartment model. This discrepancy may be explained by the fact that our two-compartment model disregards exchange processes (permeation, diffusion, and perfusion) between different parts of an inhomogeneous lesion. The model parameter k_{el} has to be interpreted, therefore, as a descriptive fit parameter. The estimation of the tissue-specific parameter k_{21}, however, is not affected by this inadequacy, since the influence of the parameter k_{el} is largely negligible during the wash-in phase (τ, $T_{21} << |T_{el}|$), from which the parameter k_{21} is estimated (cf. Eq. 4b).

To include exchange processes between different parts of an inhomogeneous lesion into the data analysis, the complexity of the pharmacokinetic model, in particular the number of compartments, must be increased. On statistical grounds, however, it is difficult to justify more than two or at least three compartments (24). As a consequence, simplifications are unavoidable in pharmacokinetic modeling. "It is essential to remember that pharmacokinetic models are not the system itself, but rather an abstraction of it that emphasizes those aspects which the investigator feels to be important. The major contribution of a suitable model is that it allows the investigator to apply mathematical techniques" (23).

Independently of whether the computed pharmacokinetic parameters can be fully explained in a physiological sense, the model given by Eq. 9 provides a very useful way to accurately parameterize the MR signal enhancement during and after intravenous Gd-DTPA infusion. Using the data analysis discussed, the complete tissue-specific information contained in a signal-time curve is condensed to two parameters: the amplitude A reflecting the degree of MR signal enhancement and the rate constant k_{21} characterizing perfusion and vascular permeability of the lesion. Doing the analysis pixel by pixel reveals the kinetic tissue properties without losing the spatial information of the MR images.

Acknowledgment: We thank Dr. Friedemann Gückel, Dr. Markus Müller-Schimpfle, and Dr. Bernd Wowra for help and referral of patients. We also thank Thomas Koch for his support in preparing the manuscript.

REFERENCES

1. Price AC, Runge VM, Allen JH. Tumor imaging with Gd-DTPA. In: Partain CL, Price RR, Patton JA, Kulkarni MV, James AE, eds. *Magnetic resonance imaging*. Philadelphia: WB Saunders, 1988:169–81.
2. Young SW, Turner RJ, Castellino RA. A strategy for the contrast enhancement of malignant tumors using dynamic computed tomography and intravascular pharmacokinetics. *Radiology* 1980;137:137–47.
3. Fike JR, Cann CE. Contrast medium accumulation and washout in canine brain tumors and irradiated normal brain: a CT study of kinetics. *Radiology* 1984;151:115–20.
4. Flower MA, Husband JE, Parker RP. A preliminary investigation of dynamic transmission computed tomography for measurements of arterial flow and tumour perfusion. *Br J Radiol* 1985;58:983–8.
5. Michael AS, Mafee MF, Valvassori GE, Tan WS. Dynamic computed tomography of the head and neck: differential diagnostic value. *Radiology* 1985;154:413–9.
6. Hopper JL, Davis SM, Tress BM, Kaye AH, Rossiter SC, Derrick PL. Analysis of dynamic computed tomography scan brain images. *Invest Radiol* 1987;22:651–7.
7. Graif M, Bydder GM, Steiner RE, Niendorf P, Thomas DGT, Young IR. Contrast-enhanced MR imaging of malignant brain tumors. *AJNR* 1985;6:855–62.
8. Koschorek F, Jensen HP, Terwey B. Dynamic MR imaging: a further possibility for characterizing CNS lesions. *AJNR* 1987;8:259–62.
9. Rosen BR, Belliveau JW, Chien D. Perfusion imaging by nuclear magnetic resonance. *Magn Res Q* 1989;5:263–81.

10. Solomon I. Relaxation processes in a system of two spins. *Phys Rev* 1955;99:559–65.
11. Bloembergen N. Proton relaxation times in paramagnetic solutions. *J Chem Phys* 1957;27:572–3.
12. Morgan LO, Nolle AW. Proton spin relaxation in aqueous solutions of paramagnetic ions. II. Cr^{+++}, Mn^{++}, Ni^{++}, Cu^{++}, and Gd^{+++}. *J Chem Phys* 1959;31:365–8.
13. Runge VM, Clanton JA, Price AC, et al. Paramagnetic contrast agents in magnetic resonance imaging: research at Vanderbilt University. *Physiol Chem Phys* 1984;16:113–22.
14. Gadian DG, Payne JA, Bryant DJ, Young IR, Carr DH, Bydder GM. Gadolinium-DTPA as a contrast agent in MR imaging—theoretical projections and practical observations. *J Comput Assist Tomogr* 1985;9:242–51.
15. Goldstein EJ, Burnett KR, Hansell JR, et al. Gadolinium DTPA (an NMR proton imaging contrast agent): chemical structure, paramagnetic properties and pharmacokinetics. *Physiol Chem Phys* 1984;16:97–104.
16. Strich G, Hagan PL, Gerber KH, Slutsky RA. Tissue distribution and magnetic resonance spin lattice relaxation effects of gadolinium-DTPA. *Radiology* 1985;154:723–6.
17. Koenig SH, Spiller M, Brown RD, III, Wolf GL. Relaxation of water protons in the intra- and extracellular regions of blood containing Gd(DTPA). *Magn Res Med* 1986;3:791–5.
18. Brasch RC, Weinmann HJ, Wesbey GE. Contrast-enhanced NMR imaging: animal studies using gadolinium-DTPA complex. *AJR* 1984;142:625–30.
19. Gries H, Miklautz H. Some physicochemical properties of the gadolinium-DTPA complex: a contrast agent for MRI. *Physiol Chem Phys* 1984;16:105–12.
20. Weinmann HJ, Laniado M, Mützel W. Pharmacokinetics of GdDTPA/dimeglumine after intravenous injection into healthy volunteers. *Physiol Chem Phys* 1984;16:167–72.
21. Weinmann HJ, Brasch RC, Press WR, Wesbey GE. Characteristics of gadolinium-DTPA complex: a potential NMR contrast agent. *AJR* 1984;142:619–24.
22. Weinmann HJ. Schering, data on file.
23. Wagner JG. *Fundamentals of clinical pharmacokinetics*. Hamilton, Ont: Drug Intelligence Publications, 1975.
24. Collins JM, Dedrick RL. Pharmacokinetics of anticancer drugs. In: Chabner BA, ed. *Pharmacologic principles of cancer treatment*. Philadelphia: WB Saunders, 1982:77–99.
25. Marquart DW. An algorithm for least squares estimation of non-linear parameters. *J Soc Indust Appl Math* 1963;11:431–41.
26. Sage MR. Blood-brain barrier. Phenomenon of increasing importance to the imaging clinician. *AJR* 1982;33:435–8.
27. Tofts PS, Kermode AG. Measurement of the blood-brain barrier permeability and leakage space using dynamic MR imaging—1. Fundamental concepts. *Magn Res Med* 1991;17:357–67.
28. Larsson HBW, Stubgaard M, Frederiksen JL, Jensen M, Henriksen O, Paulson OB. Quantitation of blood-brain barrier defect by magnetic resonance imaging and gadolinium-DTPA in patients with multiple sclerosis and brain tumors. *Magn Res Med* 1990;16:117–31.